sustainability

MDPI

Article

Remote Sensing-Based Quantitative Assessment and Spatiotemporal Analysis of Urban Heat Island Effects and Their Implications for Sustainable Urban Development in Yinchuan City

Shanshan You, Yuxin Wang and Linbo Bai *

College of Geography and Planning, Ningxia University, Yinchuan 750021, China; 15020051801@163.com (S.Y.); 18791423434@163.com (Y.W.)

* Correspondence: bailb2592@nxu.edu.com; Tel.: +86-139-9540-2592

Abstract

Utilizing MODIS LST data from 2003 to 2024, in conjunction with multi-source remote sensing data including DEM, land use, NDVI, and nighttime lights, this study conducts a remote sensing quantitative assessment and spatiotemporal characteristic analysis of the urban heat island (UHI) effect in Yinchuan City. An improved urban-rural dichotomy approach was adopted to select rural background areas, and elevation correction of land surface temperature was performed based on the zonal ordinary least squares (OLS) regression to eliminate systematic errors caused by topographic differences. The results show that: (1) From 2003 to 2024, the overall intensity of the UHI in Yinchuan City showed a slight downward trend, while the UHI area continued to expand, presenting the characteristics of "decreasing intensity and expanding scope"; (2) The UHI exhibited concentrated and contiguous distribution in summer, and the cold island phenomenon was significant in winter, reflecting the typical seasonal contrast between summer and winter; (3) The global Moran's I value increased from 0.39 to 0.82, indicating a significant enhancement in the spatial agglomeration of the UHI; (4) The standard deviation ellipse analysis revealed that the centroid of the UHI migrated toward the westward as a whole, which was consistent with the main axis of urban construction. The research results reveal the long-term evolution law and spatial pattern characteristics of the UHI effect in Yinchuan City, and provide a scientific reference for ecological planning and thermal environment regulation of cities in arid regions. These findings enhance the understanding of long-term urban thermal environment dynamics and provide important scientific support for sustainable urban planning, climate adaptation, and ecological management in arid regions. The study contributes to the quantitative monitoring of urban environmental sustainability and supports sustainable development goals related to climate action and sustainable cities.

Keywords: urban heat island effect; remote sensing quantitative assessment; LST; urban sustainability; sustainable urban development; climate adaptation; spatial autocorrelation; Yinchuan City

Check for updates

Academic Editor: Luca Evangelisti

Received: 10 March 2026
Revised: 1 April 2026
Accepted: 7 April 2026
Published: 12 April 2026

Copyright: © 2026 by the authors. Licensee MDPI, Basel, Switzerland. This article is an open access article distributed under the terms and conditions of the Creative Commons Attribution (CC BY) license.

1. Introduction

In recent decades, global urbanization has advanced rapidly, leading to drastic changes in land use and land cover patterns. The expansion of urban artificial surfaces has disturbed the surface energy balance and hydrothermal cycles, making local climate effects increasingly prominent [1]. Among these, the Urban Heat Island (UHI) effect is the most typical

manifestation. The UHI effect not only increases urban energy consumption by altering local microclimates but also significantly threatens the public health of urban residents and undermines ecosystem services [2]. As highlighted by Piracha and Chaudhary [3], the intensified urban heat significantly boosts the cooling load of buildings, leading to a spike in electricity demand during peak hours. Furthermore, these elevated temperatures pose severe physiological challenges, increasing the incidence of heat-related illnesses and mortality among vulnerable urban populations. Simultaneously, it alters local meteorological conditions, promotes photochemical reactions and ozone pollution, and further deteriorates air quality by transporting surrounding pollutants through updrafts [4].

Quantitative monitoring and dynamic analysis are the core components of urban heat island (UHI) research [5]. Regarding monitoring methods, the field has evolved from "point-based" to "surface-based" observations. Early studies primarily relied on limited ground meteorological stations to characterize urban-rural temperature differences [6,7]. Although Zhang et al. (2024) demonstrated the unique advantages of automatic weather stations in capturing fine-grained temporal rhythms, such as "stronger at night than during the day" and "stronger in summer than in winter," their sparse spatial distribution limits the revelation of continuous spatial heterogeneity in thermal fields [8]. In contrast, remote sensing, with its high temporal frequency, wide spatial coverage, and accessibility [9], has become a pivotal means for continuous spatial monitoring and addressing the coverage gaps of station-based observations [10–12]. Regarding spatiotemporal analysis, quantitative assessment has shifted from macro-trends to refined pattern characterization: Lai et al. (2021) and Liu et al. (2015) systematically revealed the complexity of UHI intensity across diurnal and seasonal cycles and its sensitivity to meteorological factors [13,14]. Meanwhile, through geo-information Tupu methods [15] and UHI intensity grading [4,16], researchers have achieved quantitative and graphical expressions of UHI spatial expansion processes. Furthermore, multi-scale explorations of driving mechanisms have intensified, confirming that the urban-rural vegetation cover difference (ΔEVI), land surface indices (NDBI, NDVI, MNDWI), and urban spatial morphology are critical factors influencing thermal distribution [17–20], while further clarifying the "sink" landscape cooling effect of wetlands [20–23]. However, existing research still exhibits certain limitations: first, the research scale in arid oasis cities of Northwest China is imbalanced, being highly concentrated in core cities like Urumqi, leaving many other oasis cities unexplored [24]. Second, due to the uniqueness of the background underlying surfaces (e.g., bare land, Gobi) in arid regions, the UHI response thresholds differ significantly from those in humid regions [22,25]. Finally, the coordination of spatiotemporal scales in multi-source data integration often leads to information loss or misinterpretation of UHI patterns [2], and interference from the lapse rate caused by complex topography frequently results in the systematic overestimation of UHI intensity in arid regions [20,26,27].

To address the aforementioned research gaps, this study selects Yinchuan—the only "International Wetland City" in Northwest China—as a representative case. Situated between the Yellow River and the Helan Mountains, Yinchuan's complex natural background, interlaced with continuous urban expansion and ecological restoration projects, provides a unique laboratory for exploring the thermal effects of urbanization. This study aims to analyze the spatiotemporal differentiation characteristics of the UHI effect in Yinchuan, with academic innovations and improvements manifested as follows: ① In terms of data consistency and methodological reliability, addressing the scale conversion errors in multi-source integration [2], this study utilizes single-source MODIS LST data from 2003 to 2024 via the Google Earth Engine (GEE) platform [28]. This ensures longitudinal consistency in sensor parameters and retrieval algorithms, effectively capturing the non-linear evolutionary trajectories of the thermal environment. ② Regarding regional specificity, this study fills

the gap in the uneven distribution of research across Northwest oasis cities, focusing on the unique UHI evolutionary patterns under the complex "wetland-oasis-desert" background of Yinchuan, thereby supplementing research in similar complex regions [24]. ③ In terms of refined assessment and comprehensive correlation analysis, in response to the trend of mechanism coupling [29], this study improves the urban-rural dichotomy for background extraction and incorporates topographic correction [26,27] to eliminate topographic interference. Furthermore, multi-source geospatial data, including land use (LUCC), vegetation abundance (NDVI), digital elevation models (DEM), and nighttime lights (NTL), are integrated for a comprehensive correlation analysis. The findings of this study aim to reveal the driving logic of the thermal environment in arid oasis cities, providing a reference for the scientific application of green and blue space infrastructure in future urbanization strategies. By integrating green and blue spaces into urban planning policies to mitigate adverse UHI effects [30], this research seeks to enhance the urban climate resilience of such ecologically fragile regions.

2. Data Collection

2.1. Study Area

Yinchuan City is located in the north-central part of the Ningxia Hui Autonomous Region in Northwest China. It is situated in the middle of the Ningxia Plain and the upper reaches of the Yellow River, adjacent to Wuzhong City to the south and Shizuishan City to the north, with a total area of approximately 9025 square kilometers. The terrain is higher in the west and lower in the east, bordered by the Helan Mountains to the west and the Yellow River to the east, forming a geomorphic pattern characterized by the staggered distribution of mountains, alluvial plains, and lake wetlands (Figure 1). Yinchuan has a temperate continental climate with four distinct seasons, abundant sunshine, and strong evaporation. The annual average temperature is 10.6 °C, the annual precipitation is 214.2 mm, and the annual sunshine duration is approximately 2740 h [31].

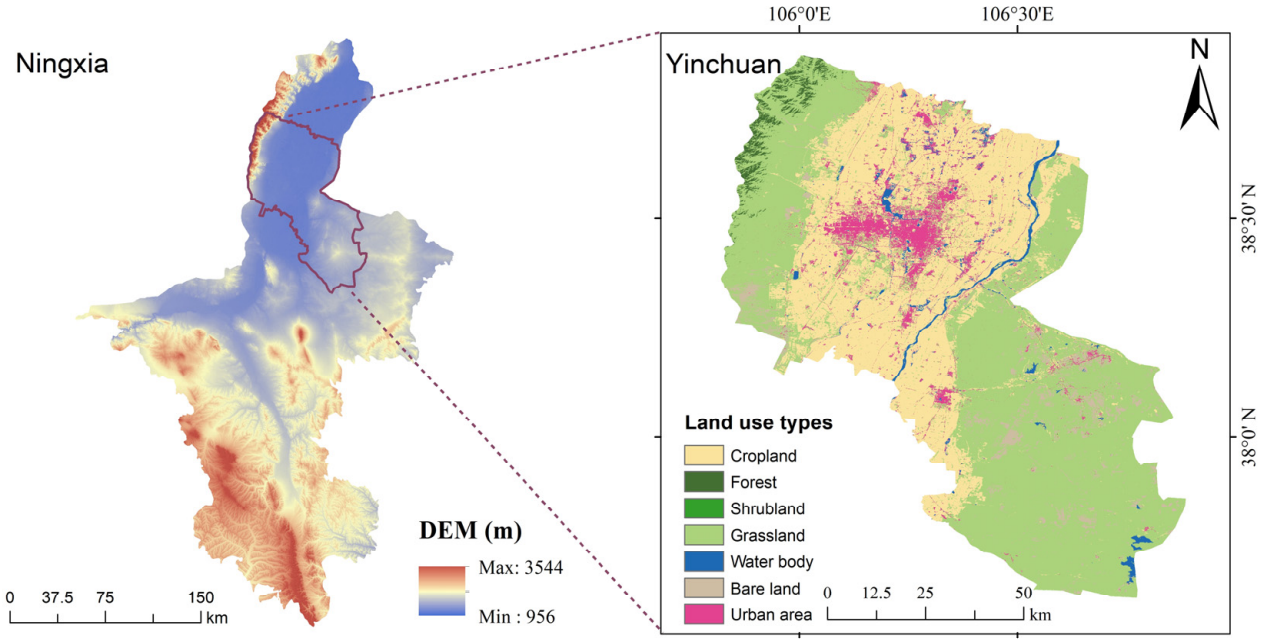


Figure 1. Location map of Yinchuan City.

2.2. Data

The multi-source datasets supporting this research are summarized in Table 1. The core data include: (1) MODIS LST daily products (MOD11A1, V6.1) with a spatial resolution

of 1 km, sourced from the Google Earth Engine (GEE) platform, used for the quantitative calculation of UHI intensity. (2) ASTER GDEM digital elevation model with an original resolution of 30 m, obtained from the Geospatial Data Cloud, providing the topographic basis for elevation-based temperature correction. (3) China Land Cover Dataset (CLCD) with a 30 m resolution, originating from the research of Professors Jie Yang and Xin Huang at Wuhan University, used for urban-rural zoning and land surface characterization. (4) MODIS NDVI monthly products (MOD13A3) with a 1 km resolution, obtained via NASA Earthdata Search, utilized for rural background extraction and identification of thermal cold sources. (5) Cross-sensor calibrated nighttime light data (500 m), sourced from the Harvard Dataverse platform. This dataset integrates DMSP/OLS and NPP-VIIRS data through a sigmoid function-based fusion framework, ensuring long-term consistency for urban boundary identification. (6) Urban built-up area raster data for 2005, 2010, 2015, and 2020 with a 30 m resolution, originating from the Chinese Urban Built-up Area Dataset (CUBA, V1.0) developed by He et al. (2022) via the National Tibetan Plateau Data Center (TPDC), used for defining the source areas of the heat island effect [32].

Table 1. Metadata and sources of the multi-source datasets used in this study.

Data Type	Dataset/Product	Year	Resolution	Source
LST	MOD11A1 (V6.1)	2003–2024	1000 m	[33]
DEM	ASTER GDEM V3	2020	30 m	[34]
Land Cover	CLCD	2003–2024	30 m	[35]
NDVI	MOD13A3	2003–2024	1000 m	[36]
Nighttime Light	Fused DMSP-VIIRS	2003–2024	500 m	[37]
Built-up Area	CUBA (V1.0)	2005, 10, 15, 20	30 m	[32]

2.3. Data Preprocessing

Referring to relevant research methods [12], this study performed standardized preprocessing on multi-source data to ensure analysis accuracy. Specifically, the Google Earth Engine (GEE) cloud platform was utilized to achieve unified acquisition and processing of the long-term MODIS LST products (2003–2024). Leveraging the high-performance computing of GEE, we conducted pixel-level quality screening to remove low-confidence data and employed spatiotemporal interpolation to repair missing values, thereby constructing a continuous dataset of monthly, seasonal, and annual LST composites (Wang et al.) [38]. Furthermore, all datasets were unified into the WGS_1984_UTM_Zone_48N projection. To eliminate errors caused by scale differences, the 30 m resolution DEM, CLCD land use data, and built-up area data, as well as the 500 m resolution nighttime light data, were uniformly resampled to 1 km using the nearest neighbor method.

To account for the significant topographic influence on the thermal environment in arid regions, this study performed elevation-based spatial partitioning using DEM data. Using ArcGIS10.8 spatial analysis tools, the study area was divided into three distinct elevation zones based on specific altitudinal thresholds: <1200 m, 1200–1400 m, and >1400 m. The selection of these thresholds is grounded in the local geomorphological gradient: the 1200 m contour serves as the boundary for the core alluvial-lacustrine plain (typically 1010–1150 m) to ensure complete coverage of the urban oasis; the 1200–1400 m interval targets the piedmont proluvial fan where the terrain begins to incline; and the >1400 m threshold identifies the rocky mountain body of the Helan Mountains [39]. This partitioning established a precise spatial foundation for the subsequent zonal elevation correction of LST, effectively eliminating systematic errors caused by vertical temperature gradients. To bridge the temporal gap between the annual MODIS LST (2003–2024) and the episodic urban built-up area data, a temporal nearest-neighbor matching approach

was employed. Specifically, the built-up area extent for a representative year was used as a spatial proxy for its surrounding period; for instance, the 2005 dataset served as the reference for the 2003–2007 period, and the 2010 dataset for 2008–2012, and so forth. This ensures the spatial consistency of the urban-rural dichotomy throughout the 22-year study period while effectively capturing the phased characteristics of urban expansion.

3. Methodology

3.1. Urban-Rural Dichotomy

The urban heat island (UHI) effect reflects the difference in land surface temperature (LST) between urban areas and surrounding rural or suburban areas. The accurate definition of rural background is crucial for quantifying the Urban Heat Island (UHI) intensity, especially in arid regions where the thermal contrast between urban surfaces and surrounding barren land is complex. Referring to the dynamic urban-extent method, this study employed an improved urban-rural dichotomy to minimize the "oasis cold island" interference from peri-urban agricultural vegetation [40]. This study employs the urban-rural dichotomy to calculate the urban heat island intensity (UHII) by extracting the temperature difference between urban built-up areas and rural background areas to quantify the UHI effect.

Referring to the improved logic of Liu et al. (2017) [21] in the quantitative assessment of the heat island in the Beijing-Tianjin-Hebei urban agglomeration, and to reduce deviations caused by improper rural background selection in traditional methods, this study constructed a screening condition for rural background areas using multi-source indicators, including land use types, vegetation coverage, and nighttime light intensity, with the specific steps as follows: ① Based on the cropland type in the China Land Cover Dataset (CLCD) to ensure the background area represents natural underlying surface characteristics; ② Utilizing MODIS NDVI products to filter high vegetation coverage areas with NDVI $\geq$0.4 to exclude interference from bare land and construction land, as bare soil in arid regions often exhibits high-temperature characteristics due to low thermal inertia; ③ Combining NPP-VIIRS nighttime light data to select areas with a Digital Number (DN) value $\leq$15 (determined via Jenks natural breaks) as low-impact areas for human activity to eliminate urban light leakage. Through multi-condition superposition analysis, the distribution of rural background areas in Yinchuan City was extracted (Figure 2).

The results show that the rural background areas are mainly concentrated in the irrigated plain farmland regions along both banks of the Yellow River, especially in the Xingqing–Jinfeng–Yongning area south of the main urban district and its eastern and southeastern directions. In the eastern foothills of the Helan Mountains and the southern part of Lingwu City, the distribution of rural background is scattered or even absent due to sparse cropland, strong nighttime lights, or significant topographic relief. The extraction results exhibit good consistency with the CLCD cropland distribution, high-value NDVI regions, and low-light areas, which can effectively reflect the baseline state of the regional natural thermal environment and provide a reliable reference for the subsequent calculation of surface urban heat island intensity (Figure 2).

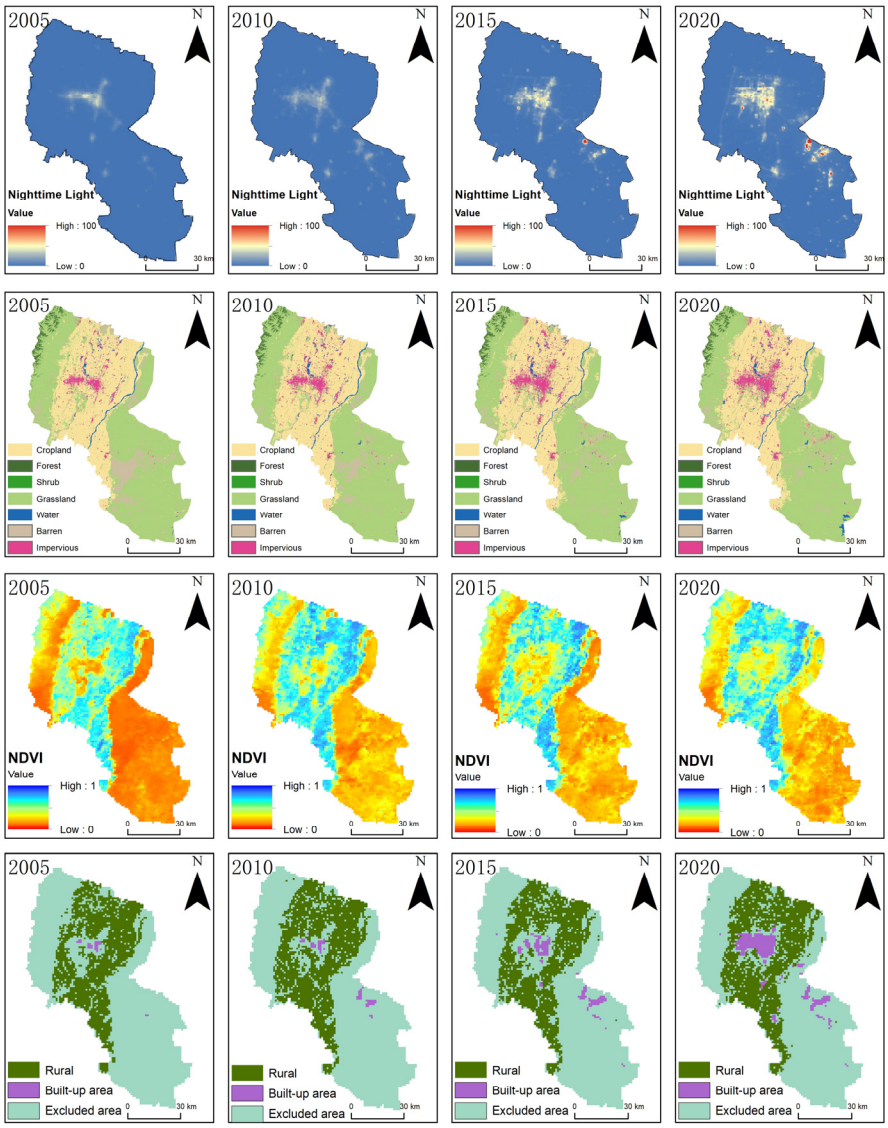


Figure 2. Urban–rural classification and rural background extraction of Yinchuan City.

3.2. Elevation Correction Model

Due to the significant vertical lapse rate of temperature in mountainous or plateau cities, raw LST data often contain topographic noise that masks the anthropogenic heat signals. Consistent with recent studies on high-density and complex terrain cities, the application of OLS regression for LST-elevation normalization is essential to decouple the natural cooling effect of altitude from the urban thermal environment [41,42]. By establishing a linear relationship between LST and elevation within each zone, the thermally representative residuals can be derived.

Yinchuan City exhibits distinct topographic variations (northern plains, central platforms, and southwestern mountains), and topographic relief has a significant impact on land surface temperature (LST). To eliminate the systematic bias caused by elevation differences, this study adopted the zonal ordinary least squares (OLS) regression method for elevation correction.

A linear relationship model was established within each elevation zone (Z_1,Z_2,Z_3):

$$T = a + bZ + \varepsilon \quad (1)$$

where T is the land surface temperature (°C); Z is the elevation; a and b are the regression coefficients; and ε is the residual term.

To obtain the optimal fitting coefficients a and b, the OLS method was used to minimize the sum of squared residuals:

$$min\sum_{i=1}^{n}(T_i - a - bZ_i)^2 \quad (2)$$

According to the principle of OLS, the analytical solutions for the regression coefficients can be obtained:

$$b = \frac{n\sum T_i Z_i - \sum T_i \sum Z_i}{n\sum Z_i^2 - (\sum Z_i)^2}, a = \overline{T} - b\overline{Z} \quad (3)$$

The formula for the corrected temperature was then derived:

$$T' = T + b(Z - \overline{Z}) \quad (4)$$

where T' is the corrected temperature (°C); and $\overline{Z}$ is the average elevation of the study area (m).

Calculation results showed that the coefficients of determination R^2 for the models in the low-altitude zone (Z_1) and mid-altitude zone (Z_2) were 0.53 and 0.54, respectively, while the R^2 in the high-altitude zone (Z_3) reached 0.87, indicating that the controlling effect of topography on temperature is more significant in high-altitude areas. The linear assumption between LST and elevation applied here is consistent with the standard environmental lapse rate principle and is widely recognized as a robust method for regional-scale topographic normalization in areas with significant terrain fluctuations [43,44]. Although the R^2 values for Z_1 and Z_2 were relatively lower, they reflect that LST in these zones is simultaneously influenced by complex surface heterogeneities and anthropogenic factors beyond elevation alone [45]. However, the primary objective of this zonal OLS correction was to eliminate the macro-scale systematic bias induced by the vertical temperature gradient rather than to achieve perfect variance fitting [44]. After correction, Moran's I of the residuals was 0.0188 ($p < 0.01$), representing an extremely weak spatial dependence. This near-zero spatial autocorrelation indicates that the systematic structural bias caused by topography has been significantly reduced, meeting the requirements for comparative UHI assessment.

3.3. Calculation of UHI Intensity

Based on the urban-rural zoning, this study calculates the land temperature difference (UHII intensity) using the following formula, referring to the urban heat island indices and classification methods proposed by Ye et al. (2011) [46]:

$$UHII_i = T_i - \frac{1}{N}\sum_{1}^{N} T_{rural} \quad (5)$$

In the formula, $UHII_i$ is the surface urban heat island intensity of the i-th grid cell (°C); T_i is the land surface temperature of the i-th grid cell in the urban built-up area (°C); and T_{rural} is the land surface temperature of the i-th grid cell in the rural background area (°C).

To quantitatively evaluate the thermal environment, the surface urban heat island intensity (SUHII) was classified into distinct grades. The classification thresholds were adopted from the scheme proposed by Ye et al. (2011) [46], which is widely recognized for its consistency with regional thermal characteristics. During the study period (2003–2024), the observed annual SUHII values in Yinchuan City ranged from −6.14 °C to +5.73 °C; this extensive range confirms that the adopted classification levels effectively capture the actual tail distribution of thermal anomalies in the region. Based on the statistical characteristics

of the land surface temperature, the classification standards for heat island intensity are set as follows (Table 2):

Table 2. Classification of Heat Island Intensity Levels.

Level	Heat Island Intensity (°C)	Meaning	Description
1	<−5	Strong Cold Island	Significant cooling areas of vegetation and water bodies
2	[−5, −2)	Relatively Strong Cold Island	Suburban areas and river valleys
3	[−2, −0)	Weak Cold Island	Urban fringe areas
4	[0, 2)	Weak Heat Island	Transition zones
5	[2, 5)	Relatively Strong Heat Island	Urban high-temperature areas
6	≥5	Strong Heat Island	Core areas of extreme high temperatures

4. Results

4.1. Temporal Evolution Characteristics

Figure 3 illustrates the interannual evolution characteristics of the urban heat island (UHI) effect in Yinchuan City from 2003 to 2024. Specifically, (a) characterizes the annual statistical distribution of heat island intensity through box plots, indicating that the heat island intensity generally enhanced with significant fluctuations between 2003 and 2010, and gradually stabilized with a slight downward trend after 2010. This transition from dramatic fluctuation to relative stability in UHI intensity has been observed in other long-term monitoring studies, suggesting that as urban structures mature, the thermal environment reaches a new equilibrium state [38]. (b) Based on the linear fitting of the heat island area, it reveals a continuous expansion of the heat island coverage (R^2 = 0.606), showing a stable growth trend. Combining the two figures, it can be observed that during the study period, the UHI in Yinchuan City presented a typical pattern of "decreasing intensity and expanding scope." This phenomenon reflects a common spatial evolution of the urban thermal environment, where the decentralized expansion of impervious surfaces leads to a broader but less concentrated thermal impact [47]. Driven by urban expansion, while the extreme intensity has moderated, the spatial extension continues to strengthen. This evolution pattern is consistent with the general characteristics of cities in the arid regions of Northwest China. Ren et al. [48] pointed out that under high aridity backgrounds, construction density and the expansion of impervious surfaces dominate the growth of the heat island range, while the construction of vegetation and wetlands can form cooling effects locally. Kim and Brown further noted that cities in different climate zones exhibit coexistence of spatial expansion and intensity fluctuations during the evolution of the heat island [49].

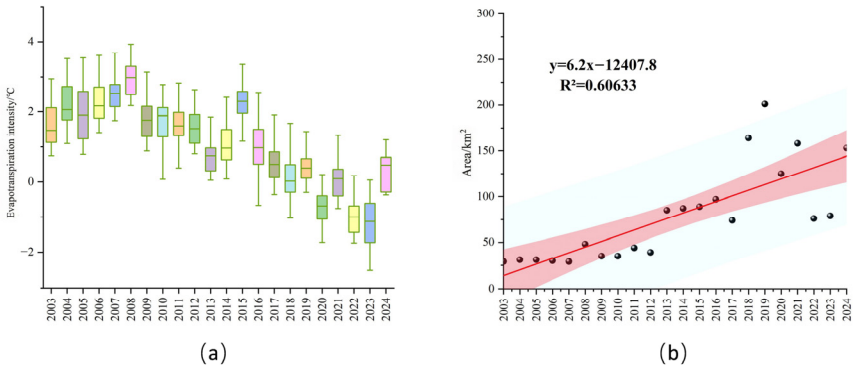


Figure 3. Interannual changes in UHII and areal extent in Yinchuan (2003−2024). (**a**) Interannual variation of urban heat island intensity (UHII) in Yinchuan, 2003−2024; (**b**) Interannual variation of urban heat island areal extent in Yinchuan, 2003−2024.

4.2. Seasonal Differentiation Characteristics

By comparing the land surface temperature (LST) distribution maps for summer and winter across four periods—2005, 2010, 2015, and 2020 (Figure 4)—it is evident that the thermal environment of Yinchuan City exhibits significant seasonal reversal characteristics. This phenomenon is deeply rooted in the seasonal shift in the surface energy balance. The urban heat island (UHI) is most prominent in summer, where the high-temperature zones have evolved from a scattered distribution in 2005 to a continuous and contiguous pattern in 2020, forming a "point-belt-patch" expansion trend. This summer intensification is primarily driven by the dominance of sensible heat flux over impervious surfaces and the high solar radiation absorption of urban canyons. The UHI core has remained stable at the junction of Xingqing, Jinfeng, and Xixia Districts and extends north and south along the main axis of urban construction. Conversely, winter is characterized by a dominant cold island distribution, with its range expanding and connectivity increasing over time. In 2005, only localized cold spots appeared around the urban area; after 2010, the cold island gradually expanded toward the periphery, forming continuous cold belts in the main urban district; by 2020, it covered large areas, creating a sharp contrast with the summer pattern. This winter reversal reflects the regional climatic constraints of an arid oasis city, where the low thermal inertia of urban materials leads to rapid long-wave radiative cooling during the shorter, colder days, often outpacing the heat retention of the sparse peripheral vegetation. Overall, Yinchuan City demonstrates a seasonal inverse response characterized by the concentrated intensification of the summer heat island and the significant expansion of the winter cold island.

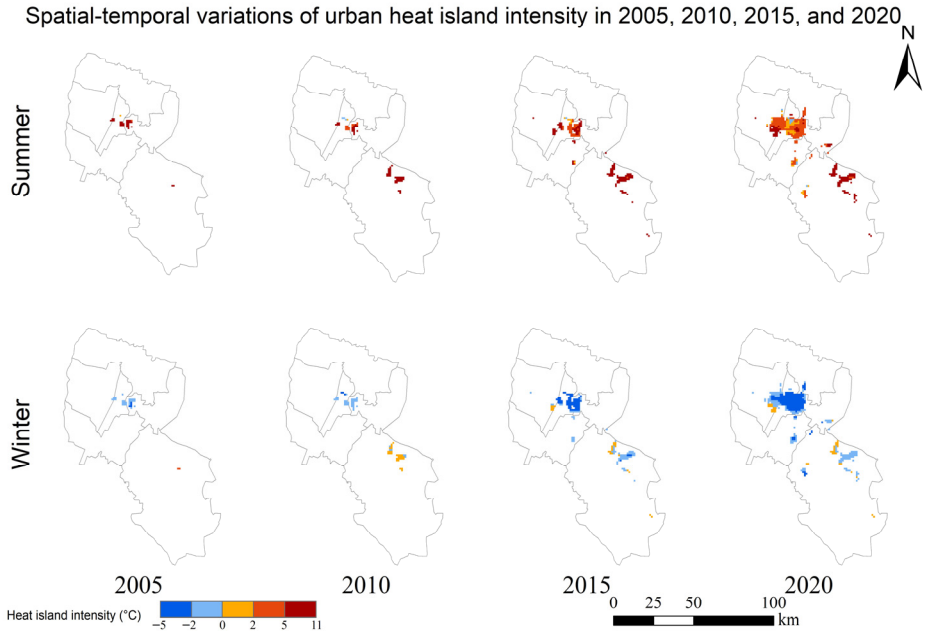


Figure 4. Seasonal maps of urban heat island changes in 2005, 2010, 2015 and 2020 (summer vs. winter).

4.3. Structural Characteristics of Heat Island Levels

The structural characteristics of heat island levels shown in Figure 5 reveal significant temporal differentiation in Yinchuan City from 2003 to 2024. Overall, from 2003 to 2008, the proportion of "Weak Heat Island" and "Relatively Strong Heat Island" remained consistently high at 50–80%, with thermal zones primarily concentrated in Xingqing and Jinfeng Districts; notably, the "Relatively Strong Heat Island" reached a periodic peak in 2007. A distinct turning point in the hierarchical structure occurred between 2009 and 2014, when the "Weak Cold Island" became the dominant level, primarily distributed in Lingwu

City, reflecting the cooling effect of the platform terrain and natural underlying surfaces. During the same period, although the main urban district maintained UHI characteristics, the thermal intensity weakened compared to the previous stage. From 2015 to 2018, the "Weak Cold Island" and "Weak Heat Island" levels alternately dominated, presenting a transitional state where the thermal environment gradually approached equilibrium; Lingwu City continued to host the main cold island distribution, while level fluctuations in the main urban district slowed down. From 2019 to 2024, the "Weak Heat Island" once again became the dominant level, with the UHI core re-concentrating in Xingqing, Jinfeng, and Xixia Districts, while Lingwu City generally maintained a cold island pattern. In summary, the UHI levels in Yinchuan City exhibited a phased evolution from "strong heat dominance" to "cold island intensification" and then to "UHI resurgence," corresponding spatially to a "main urban district—platform—main urban district" thermal transition pattern, which reflects the combined driving effects of urban expansion, topographic differences, and ecological governance.

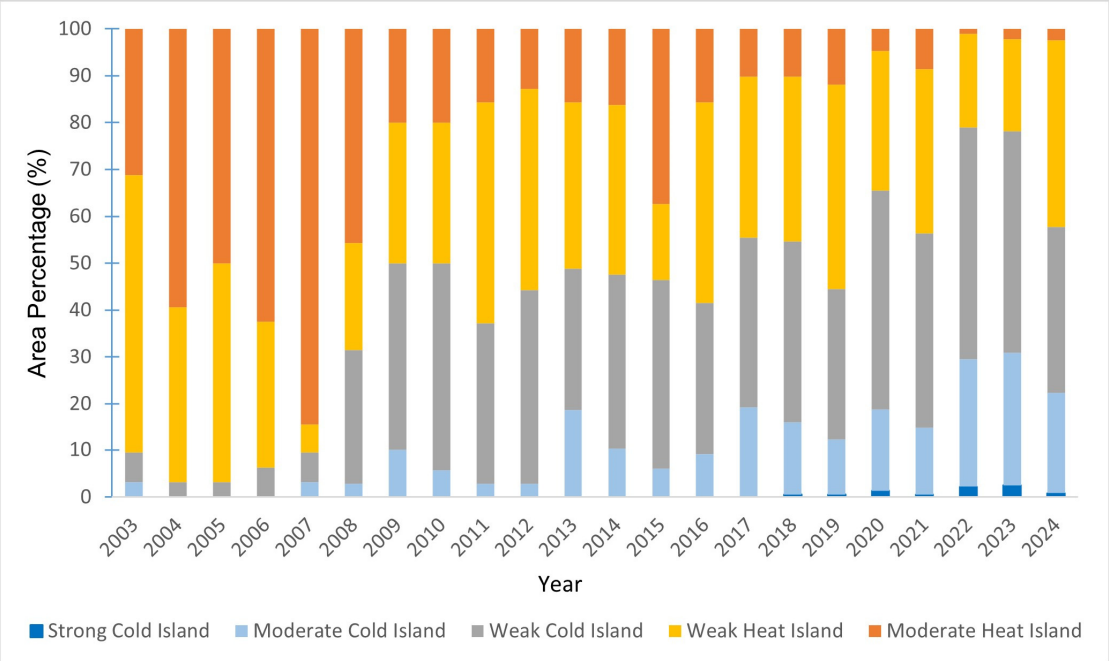


Figure 5. Changes in the proportion of different UHI levels in Yinchuan City from 2003 to 2024.

4.4. Spatial Distribution Characteristics

4.4.1. Evolution of Multi-Period Spatial Distribution

Between 2003 and 2024, the spatial pattern of the urban heat island (UHI) in Yinchuan City generally exhibited an evolutionary trend of expanding from point-like distributions to belt-like and patch-like formations (Figure 6). In the early stage (2003–2008), the heat island was primarily concentrated at the junction of Xingqing and Jinfeng Districts, manifesting as localized and isolated high-temperature patches. After 2010, with the contiguous construction of the main urban area and the expansion of roads and industrial zones, the UHI range rapidly extended outward, forming a continuous high-temperature belt along the north–south axis. Since 2020, the UHI distribution has developed a distinct "urban core–peripheral secondary" dual-layer structure. Specifically, within the main urban area, Xingqing, Jinfeng, and Xixia Districts are concentrated zones of high-intensity heat islands, while the peripheral Yongning and Helan Counties are dominated by low-intensity heat islands or cold islands. Overall, the spatial pattern of Yinchuan's UHI presents a typical evolutionary characteristic of "core intensification, peripheral extension, and regional

connectivity" in tandem with urban expansion. The continuous shift in the UHI gravity center towards the newly developed zones reflects the spatial reorganization of urban functional land use [50]. This spatial evolution pattern is consistent with the urban thermal field expansion model proposed by Voogt and Oke (2003) [11], indicating that the spatial clustering of heat islands tends to expand along the main axis of urban development and is constrained by topography and the layout of functional zones.

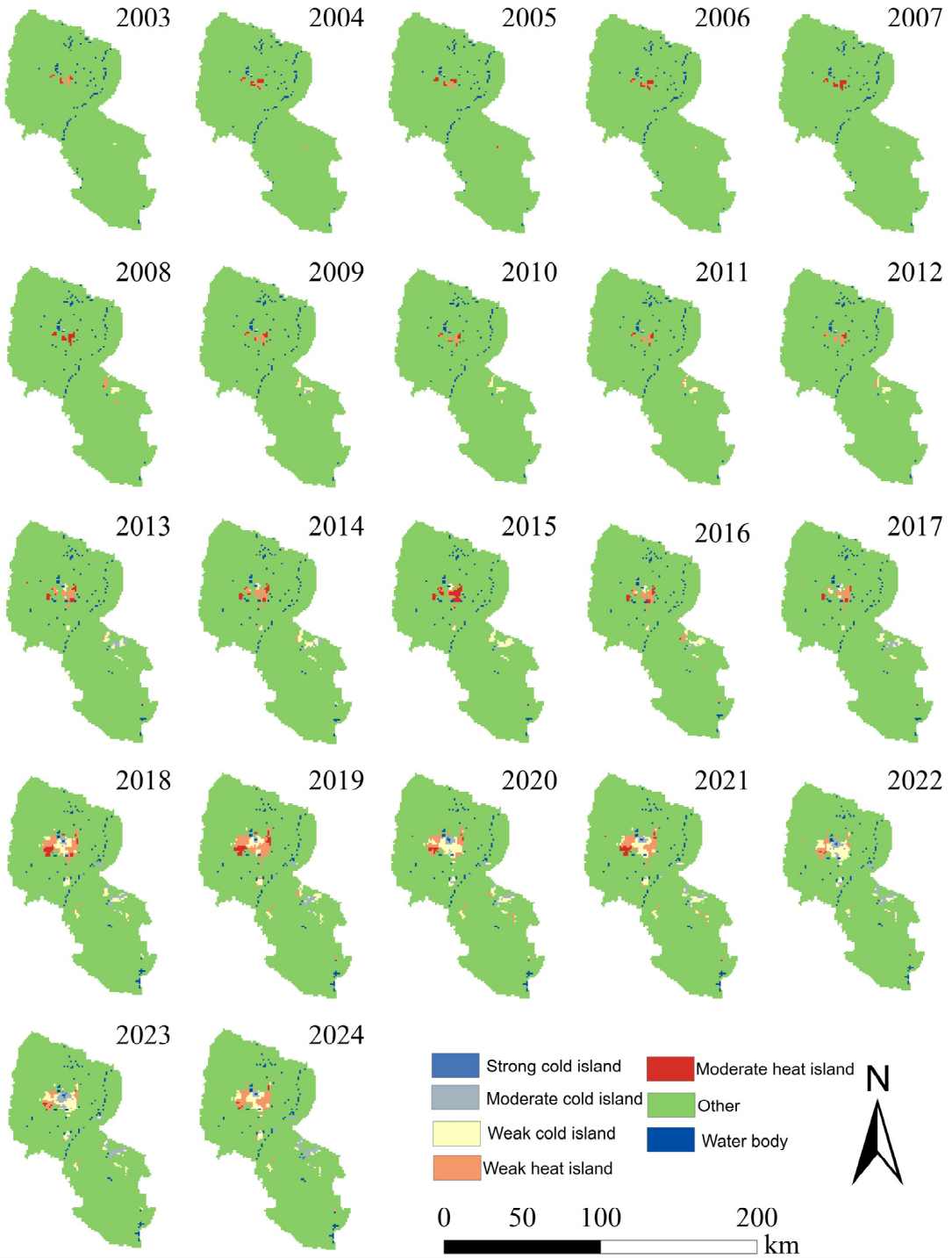


Figure 6. Spatial distribution maps of urban heat islands in Yinchuan City from 2003 to 2024.

4.4.2. Global Spatial Autocorrelation Characteristics

The Global Moran's I values reflect the overall trend of spatial clustering of the urban heat island (UHI) in Yinchuan City (Figure 7). Between 2003 and 2024, the Global

Moran's I remained at a high level and showed an overall upward trend, indicating a persistent positive spatial correlation in the distribution of the UHI. The increasing spatial autocorrelation (Moran's I) indicates a transition from fragmented "hot spots" to large-scale thermal clusters, a pattern frequently observed in high-density semi-arid urban environments [51]. Similar intensified spatial clustering phenomena have been verified in other arid region cities, such as Taiyuan (Wu, 2024) [44] and Lanzhou (Yin, 2021) [20], suggesting that the enhancement of UHI spatial agglomeration is a common manifestation in the later stages of urbanization. In the early stage (2003–2010), Moran's I gradually rose, indicating that the UHI transitioned from a dispersed distribution to significant clustering. Between 2010 and 2016, the growth slowed down, and the clustering pattern stabilized. After 2017, although there were slight fluctuations, the values generally remained within a high-value range. These results suggest that as urban construction density increases and built-up areas become more contiguous, the clustering of the UHI spatial structure gradually strengthens, while ecological restoration and wetland protection projects have only formed weak dispersion effects in localized areas.

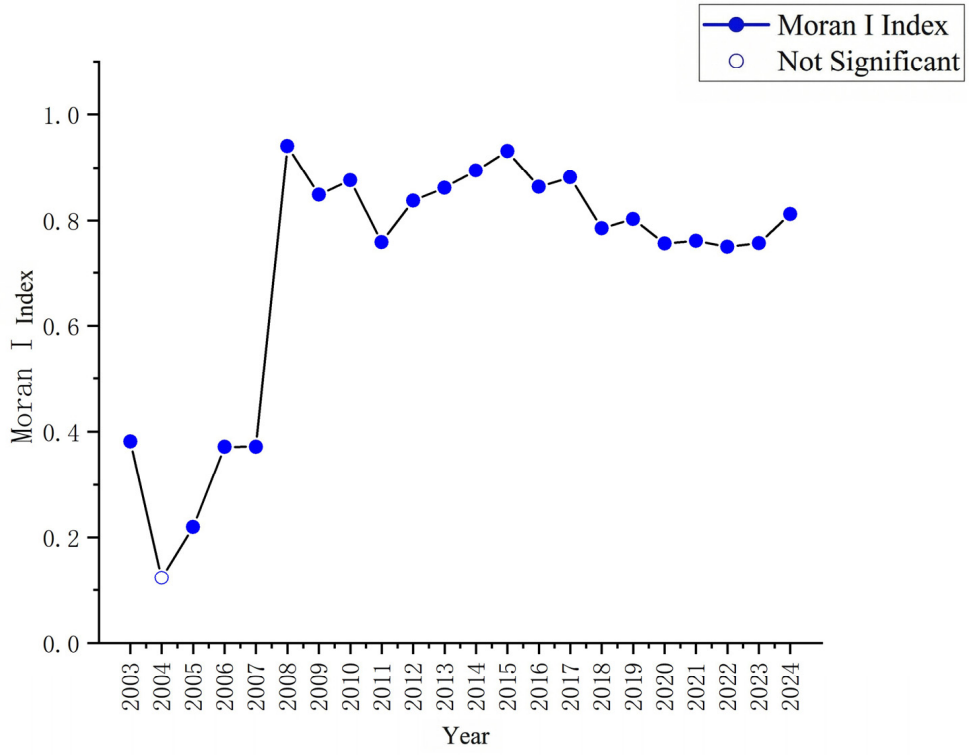


Figure 7. Interannual variation in global Moran's I for surface urban heat islands in Yinchuan City (2003–2024).

4.4.3. Local Spatial Clustering Characteristics

Based on the LISA clustering results (Figure 8), the urban heat island (UHI) in Yinchuan City exhibits significant spatial heterogeneity at the local scale. The "High-High (HH)" clusters are stably concentrated at the junction of Xingqing, Jinfeng, and Xixia Districts, representing the urban thermal core, while the "Low-Low (LL)" clusters are primarily distributed in peripheral ecological and agricultural regions. This spatial dichotomy reflects the distinctive hysteretic dynamics and water availability gradients inherent in arid oasis cities [52]. Specifically, the intensification and outward migration of HH zones along the main urban axis between 2003 and 2024 indicate that urban expansion has altered the local surface energy balance, where low-albedo impervious surfaces increasingly dominate. In contrast, the stability of LL zones in areas like Lingwu and Helan is maintained by the evaporative cooling of irrigation-dependent vegetation, which remains out of phase with

the thermal signals of the surrounding arid background [52]. As Yang et al. [22] pointed out, such local clustering effectively reveals the morphological evolution of UHIs, where HH zones correspond to core functional areas and LL zones to peripheral ecological belts. Ultimately, the intensifying clustering and increasingly evident local differentiation in Yinchuan demonstrate how background climatic constraints and anthropogenic land-use changes jointly shape the spatial structure of the SUHI.

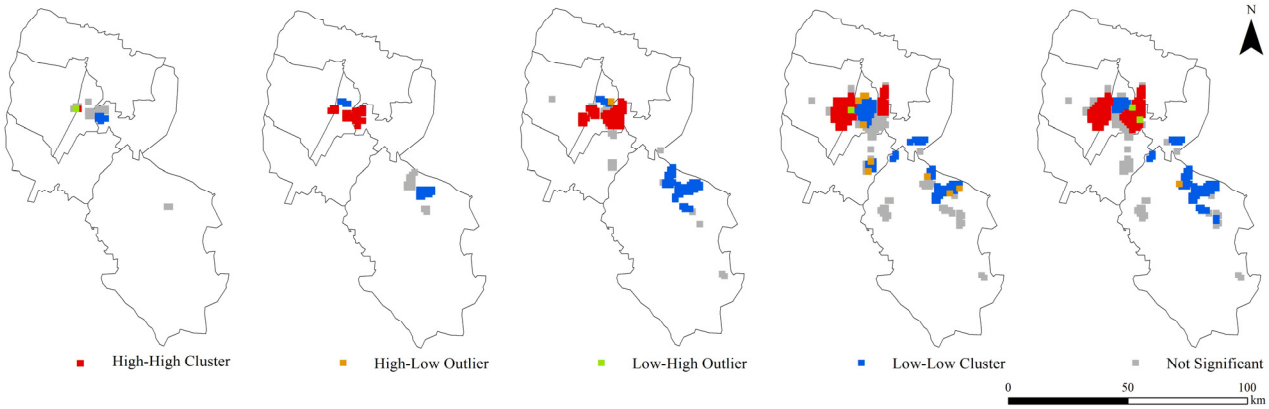


Figure 8. LISA cluster maps of urban heat islands in Yinchuan City.

4.5. Standard Deviation Ellipse and Centroid Shift

To reveal the overall spatial morphological changes and the evolution of the dominant direction of the urban heat island (UHI) in Yinchuan City, the Standard Deviation Ellipse (SDE) method was employed to conduct spatial fitting and centroid analysis for areas classified as "Relatively Strong Heat Island and above" from 2003 to 2024 (Figure 9). The results indicate that the UHI generally exhibits a Northwest–Southeast distribution pattern. During the initial stage of the study (2003–2012), the high ratio of the long axis to the short axis reflected a significant directional preference in the spatial distribution of the heat island. As urbanization intensified, the expansion rate of the short axis gradually surpassed that of the long axis, leading to a decreasing trend in the axis ratio and a more circular SDE morphology. This geometric evolution, coupled with the continuous increase in UHI coverage area, objectively records the transition of Yinchuan's thermal environment from early "axis-based ribbon expansion" to "all-around contiguous diffusion."

The characteristics of centroid migration show that from 2003 to 2024, the UHI centroid in Yinchuan generally shifted from the eastern Xingqing District toward the central Jinfeng and western Xixia Districts, aligning closely with the spatiotemporal evolution of the urban construction center. According to Bu et al. (2022) [53], Yinchuan entered a period of rapid expansion after 2008, during which the built-up area transitioned from a single-core model in Xingqing to a "connected" pattern involving Jinfeng and Xixia. This expansion mode directly drove the significant westward leap of the thermal centroid observed in this study. Furthermore, Mao et al. (2020) [54] highlighted the drastic land-use transformation in the Yinchuan Plain, specifically the large-scale conversion of cultivated land into construction land, which provides the physical basis for the thermal field's response toward newly developed areas. Wu et al. [44] also found a directional drift of the heat island centroid along the urban development axis in their study of Taiyuan, reflecting the response of the thermal environment to urban construction patterns. Kim and Brown (2021) [49] pointed out that centroid migration has become an important indicator for evaluating the long-term evolution of UHIs and can be used to quantify the degree of coupling between urban expansion and the center of gravity of the thermal field. In the early stage of the study, the centroid was located in the northwestern part of Xixia District. As construction in the main urban area progressed and functions expanded toward the east and

south, the centroid gradually shifted toward the junction of Jinfeng and Xingqing Districts. After 2020, the centroid basically stabilized at the southern fringe of the main urban area, indicating that the spatial center of the heat island core has become firm along with the urban structure. Overall, the westward migration of the centroid and the circularization of the SDE morphology accurately reflect that the UHI expansion in Yinchuan is jointly driven by urban "internal filling" expansion and the resulting changes in land surface properties.

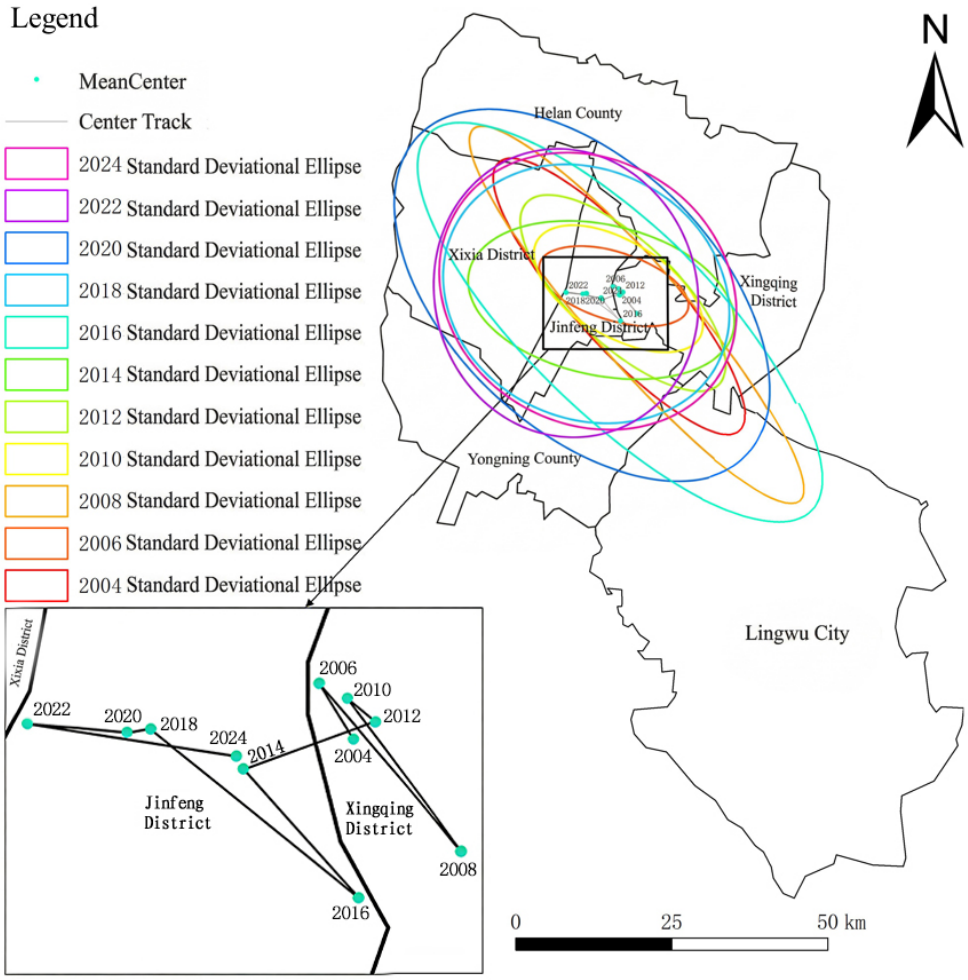


Figure 9. Standard deviation ellipses and centroid migration of strong and above UHI zones in Yinchuan City (2003–2024).

5. Conclusions and Analysis

5.1. Conclusions

Taking Yinchuan as the study area and utilizing long-term MODIS LST time-series data, this study quantitatively evaluated the Urban Heat Island (UHI) intensity levels from 2003 to 2024. Building upon the urban-rural dichotomy, we applied elevation-based surface temperature corrections to analyze the spatial-temporal dynamics of Yinchuan's thermal environment. The primary findings are as follows:

From 2003 to 2024, the urban heat island effect in Yinchuan generally exhibited a trend of "declining intensity and expanding extent." The mean heat island value rose rapidly before 2010, then stabilized and slightly decreased thereafter. Spatially, it evolved from a scattered distribution to continuous clustering, reflecting a typical thermal environment response under the background of urban expansion in arid regions.

The urban heat island in Yinchuan has a significant seasonal contrast between summer and winter: the heat island in summer has a wide range and high intensity, while cold

islands are contiguous and expanding in range during winter. The hierarchical structure of the heat island is dominated by relatively strong and weak heat islands. The area of strong heat islands rose slightly in the later period, and the proportion of cold islands has gradually recovered since 2015.

Global Moran's I values continued to rise, indicating that the spatial clustering of the heat island has gradually enhanced. LISA clustering results showed that the main urban area is the high-value aggregation core, while the peripheral areas are stable cold source zones. Standard deviational ellipse analysis showed that the main axis direction of the heat island is consistent with the direction of urban development, and the centroid has shifted westward as a whole.

The research indicates that the evolution of the heat island effect in Yinchuan is the result of the combined effects of urban expansion, topographical differences, and ecological regulation. Future efforts should start from urban spatial layout, green space system optimization, and ecological corridor construction to strengthen the regulation of the urban thermal environment and sustainable development paths in arid regions.

5.2. Discussion

This study achieves two key improvements in the quantitative remote sensing assessment of urban heat islands (UHI) in arid regions, providing a scientific basis for precision urban thermal environment management. First, an optimized "urban-rural dichotomy" scheme suitable for oasis cities was constructed. By redefining urban boundaries based on the multi-core expansion pattern of Yinchuan, this approach avoids misjudgments caused by administrative divisions. This suggests that urban planning should move beyond traditional administrative boundaries to implement "cross-district thermal equilibrium zones," specifically by monitoring heat contributions from emerging built-up areas like the Lingwu main district [44]. Second, a "belt-based elevation correction" method was proposed to mitigate the interference of elevation differences between plains and foothills on LST. The correction of the previously underestimated intensity on the Lingwu platform implies that "vertical-adaptive planning" is essential; for high-elevation platforms, building density and orientation should be strictly regulated to utilize natural topographic ventilation [43,45]. Furthermore, as Yinchuan is a typical oasis city, the ways in which green and blue space infrastructure is applied in future urban growth strategies warrant greater consideration in urban planning policy to mitigate the adverse effects of the UHI and enhance climate resilience [30]. This is particularly crucial for oasis cities where the strategic integration of existing wetland networks can leverage the high thermal capacity of water bodies to enhance evaporative cooling in high-density clusters. The workflow developed in this study is generalizable for urban climate simulation and environmental monitoring in other arid regions.

Despite these contributions, this study has limitations due to data and methodological constraints. (1) Heat island identification relies on built-up area masking; rapid urban expansion and special landforms, such as the Lingwu platform, may lead to a relatively weak representation of local heat islands. (2) The 1 km resolution of MODIS data makes it difficult to characterize the thermal environment at the neighborhood scale, easily underestimating fine-grained temperature differences in the transition zones between oases, plains, and platforms. (3) This research focuses on spatial-temporal pattern analysis, with insufficient quantitative decomposition of driving mechanisms. Although elevation correction improves the rationality of urban-rural comparisons, the comprehensive influence of multiple factors—such as urban morphology, vegetation structure, and water body characteristics—requires further in-depth exploration in the future using high-resolution remote sensing and multi-source data.

Author Contributions: Conceptualization, S.Y.; Methodology, S.Y.; Data curation, S.Y. and Y.W.; Writing—original draft, S.Y.; Writing—review and editing, L.B.; Visualization, S.Y. and Y.W.; Supervision, L.B.; Project administration, L.B.; Funding acquisition, L.B. All authors have read and agreed to the published version of the manuscript.

Funding: This research was funded by the Major Projects of the Ningxia Natural Science Foundation, grant number [2023BEG02043].

Institutional Review Board Statement: Not applicable.

Informed Consent Statement: Not applicable.

Data Availability Statement: No new data were created or analyzed in this study.

Conflicts of Interest: The authors declare no conflict of interest.

References

1. Reiners, P.; Sobrino, J.; Kuenzer, C. Satellite-Derived Land Surface Temperature Dynamics in the Context of Global Change—A Review. *Remote Sens.* **2023**, *15*, 1857. [CrossRef]
2. Zhao, L.; Fan, X.; Hong, T. Urban Heat Island Effect: Remote Sensing Monitoring and Assessment—Methods, Applications, and Future Directions. *Atmosphere* **2025**, *16*, 791. [CrossRef]
3. Piracha, A.; Chaudhary, M.T. Urban Air Pollution, Urban Heat Island and Human Health: A Review of the Literature. *Sustainability* **2022**, *14*, 9234. [CrossRef]
4. Wang, Y.N. Research on Urban Heat Island Effect Analysis Based on Remote Sensing Images. *Surv. Spat. Geoinform.* **2025**, *48*, 75–77.
5. Peng, J.; Ma, J.; Liu, Q.; Liu, Y.; Hu, Y.; Li, Y.; Yue, Y. Spatial-Temporal Change of Land Surface Temperature across 285 Cities in China: An Urban-Rural Contrast Perspective. *Sci. Total Environ.* **2018**, *635*, 487–497. [CrossRef]
6. Shang, J.S.; Li, B.L.; Sun, X.L.; Xia, B.X. Analysis of Summer Urban Heat Island Effect Characteristics in Jinan. *Arid Meteorol.* **2018**, *36*, 70–74.
7. Jin, L.N.; Li, X.F. Analysis of Fine Spatio-temporal Characteristics of Urban Heat Island and Cold Island in Xi'an from 2014 to 2017. *Desert Oasis Meteorol.* **2021**, *15*, 97–102.
8. Zhang, D.Y.; Shen, Z.; Wang, D.P.; Wang, M. Research and Analysis of Nanjing Urban Heat Island Effect Characteristics from 2017 to 2022. *Meteorol. Hydrol. Mar. Instrum.* **2024**, *41*, 67–69. [CrossRef]
9. Ren, X.J.; Li, G.D.; Liu, M.; Li, P.F. Current Status and Prospects of Research Methods for Urban Heat Island Effect. *J. Henan Univ. (Nat. Sci.)* **2022**, *52*, 290–304. [CrossRef]
10. Ayanlade, A.; Jegede, O.O. Evaluation of the Intensity of the Daytime Surface Urban Heat Island: How Can Remote Sensing Help? *Int. J. Image Data Fusion* **2015**, *6*, 348–365. [CrossRef]
11. Voogt, J.A.; Oke, T.R. Thermal Remote Sensing of Urban Climates. *Remote Sens. Environ.* **2003**, *86*, 370–384. [CrossRef]
12. Weng, Q. Thermal Infrared Remote Sensing for Urban Climate and Environmental Studies: Methods, Applications, and Trends. *ISPRS J. Photogramm. Remote Sens.* **2009**, *64*, 335–344. [CrossRef]
13. Lai, J.; Zhan, W.; Voogt, J.; Quan, J.; Huang, F.; Zhou, J.; Bechtel, B.; Hu, L.; Wang, K.; Cao, C.; et al. Meteorological Controls on Daily Variations of Nighttime Surface Urban Heat Islands. *Remote Sens. Environ.* **2021**, *253*, 112198. [CrossRef]
14. Liu, Y.H.; Luan, Q.Z.; Quan, W.J.; Zhang, S. Research on the Thermal Environment of the Beijing-Tianjin-Tangshan City Cluster Based on Multi-source Satellite Data. *Ecol. Environ. Sci.* **2015**, *24*, 1150–1158. [CrossRef]
15. Wu, X.W.; Xu, Y.M.; Gong, W.F. Graphical Information Feature Analysis of the Spatial Pattern and Changes of Urban Heat Islands. *Geomat. Inf. Sci. Wuhan Univ.* **2017**, *42*, 1711–1718. [CrossRef]
16. Pan, W.W. Application of Remote Sensing Image Processing Technology in the Research of Urban Heat Island Effect. *Surv. World* **2021**, 50–54.
17. Liu, C.X.; Wang, L.Q.; Xu, X.; Zhang, S.H.; Zhang, Z.Q. Impact of Vegetation Coverage on Summer Urban Heat Island Effect in China from 2001 to 2021. *Acta Ecol. Sin.* **2024**, *44*, 11020–11034. [CrossRef]
18. Huang, Q.F. Research Progress on Multi-scale Effects of Urban Spatial Morphology on the Urban Heat Island Effect. *Sci. Geogr. Sin.* **2021**, *41*, 1832–1842. [CrossRef]
19. Weng, Q.; Lu, D.; Schubring, J. Estimation of Land Surface Temperature–Vegetation Abundance Relationship for Urban Heat Island Studies. *Remote Sens. Environ.* **2004**, *89*, 467–483. [CrossRef]
20. Yin, K.K.; Wei, G.J.; Hu, Y.X.; Chen, H.P. Quantitative Analysis of Urban Heat Island Effect and Surface Index in Lanzhou. *Sci. Surv. Mapp.* **2017**, *42*, 55–60. [CrossRef]

21. Liu, Y.H.; Fang, X.Y.; Zhang, S.; Luan, Q.Z.; Quan, W.J. Quantitative Assessment of Urban Heat Island in Beijing-Tianjin-Hebei Urban Agglomeration. *Acta Ecol. Sin.* **2017**, *37*, 5818–5835.
22. Yang, H.; Wang, X.F.; Zhang, S.L.; Li, X. Variation Characteristics of Urban Heat Island Effect and Its Response to Urban Expansion in Gansu Province. *Remote Sens. Technol. Appl.* **2025**, *40*, 110–121.
23. Xiang, X.Y.; Du, J.; Song, K.S.; Zhao, B.Y.; Zhou, H.H.; Guo, P.P.; Zhang, L.Y.; Hu, Y.T. Remote Sensing Analysis of the Impact of Wetlands on the Heat Island Effect in Fuzhou. *J. Earth Environ.* **2021**, *12*, 411–424.
24. Fan, J.Y.; Chen, X.G.; Sun, J.X. Research Progress on Urban Heat Island Effect of Oasis Cities in the Arid Region of Northwest China. *Environ. Prot. Sci.* **2024**, *50*, 9–18, 31. [CrossRef]
25. Clinton, N.; Gong, P. MODIS Detected Surface Urban Heat Islands and Sinks: Global Locations and Controls. *Remote Sens. Environ.* **2013**, *134*, 294–304. [CrossRef]
26. Zhang, D.J.; Yang, S.Q.; Zhu, H.; Ye, Q.Y.; He, Z.N.; Rao, Z.J. Quantitative Evaluation of Heat Island Effect in the Urban Core Area of Chongqing. *J. Appl. Meteorol. Sci.* **2023**, *34*, 91–103.
27. Liu, S.H.; Cao, Y.G.; Jia, Y.H.; Zhou, T.X.; Zhou, S.H. Research Progress on Urban Heat Island Effect. *Anhui Agric. Sci. Bull.* **2019**, *25*, 117–121. [CrossRef]
28. Ravanelli, R.; Nascetti, A.; Cirigliano, R.V.; Di Rico, C.; Leuzzi, G.; Monti, P.; Crespi, M. Monitoring the Impact of Land Cover Change on Surface Urban Heat Island through Google Earth Engine: Proposal of a Global Methodology, First Applications and Problems. *Remote Sens.* **2018**, *10*, 1488. [CrossRef]
29. Liu, J.C.; Yin, L.; Zhang, B.L. Research Progress of Urban Heat Island Effect at Home and Abroad. *J. Shandong Norm. Univ. (Nat. Sci.)* **2025**, *40*, 21–35.
30. Gunawardena, K.R.; Wells, M.J.; Kershaw, T. Utilising Green and Bluespace to Mitigate Urban Heat Island Intensity. *Sci. Total Environ.* **2017**, *584–585*, 1040–1055. [CrossRef]
31. Yinchuan Municipal Bureau of Statistics. Yinchuan Statistical Yearbook 2024. Available online: https://tjj.yinchuan.gov.cn/tjsj/ndsj/ (accessed on 2 May 2025).
32. He, C. *Dataset of Urban Built-Up Area in China (1992–2020)*; CASEarth Thematic Data System: Beijing, China, 2022; Volume 1.0.
33. Wan, Z.; Hook, S.; Hulley, G. *MODIS/Terra Land Surface Temperature/Emissivity Daily L3 Global 1km SIN Grid V061*; NASA Land Processes Distributed Active Archive Center: Sioux Falls, SD, USA, 2021.
34. Geospatial Data Cloud. Available online: https://www.gscloud.cn/sources/accessdata/310?pid=302 (accessed on 2 April 2025).
35. Yang, J.; Huang, X. The 30 m Annual Land Cover Datasets and Its Dynamics in China from 1990 to 2020. *Earth Syst. Sci. Data* **2021**, *13*, 3907–3925. [CrossRef]
36. MODIS/Terra Vegetation Indices Monthly L3 Global 1km SIN Grid V061. Available online: https://search.earthdata.nasa.gov/search/granules?p=C2327962326-LPCLOUD (accessed on 2 April 2025).
37. Chen, Z.; Yu, B.; Yang, C.; Zhou, Y.; Yao, S.; Qian, X.; Wang, C.; Wu, B.; Wu, J.; Liao, L.; et al. The Global NPP-VIIRS-like Nighttime Light Data (Version 2) for 1992–2024. *Harv. Dataverse Dataset* **2020**, 304. [CrossRef]
38. Wang, M.; Lu, H.; Chen, B.; Sun, W.; Yang, G. Fine-Scale Analysis of the Long-Term Urban Thermal Environment in Shanghai Using Google Earth Engine. *Remote Sens.* **2023**, *15*, 3732. [CrossRef]
39. Natural Geography_Yinchuan Municipal People's Government. Available online: https://yinchuan.gov.cn/sshc/ycgk/zrdl/ (accessed on 30 March 2026).
40. Si, M.; Li, Z.-L.; Nerry, F.; Tang, B.-H.; Leng, P.; Wu, H.; Zhang, X.; Shang, G. Spatiotemporal Pattern and Long-Term Trend of Global Surface Urban Heat Islands Characterized by Dynamic Urban-Extent Method and MODIS Data. *ISPRS J. Photogramm. Remote Sens.* **2022**, *183*, 321–335. [CrossRef]
41. Qiao, Z.; Jia, R.; Liu, J.; Gao, H.; Wei, Q. Remote Sensing-Based Analysis of Urban Heat Island Driving Factors: A Local Climate Zone Perspective. *IEEE J. Sel. Top. Appl. Earth Obs. Remote Sens.* **2024**, *17*, 17337–17348. [CrossRef]
42. Lin, S.; Du, J.; Fan, J. Spatio-Temporal Evolution of Surface Urban Heat Island Distribution in Mountainous Urban Areas Based on Local Climate Zones: A Case Study of Tongren, China. *Sustainability* **2025**, *17*, 8744. [CrossRef]
43. Xue, Y.; Zhu, X.; Wu, Z.; Duan, S.-B. Retrieval of Land Surface Temperature over Mountainous Areas Using Fengyun-3D MERSI-II Data. *Remote Sens.* **2023**, *15*, 5465. [CrossRef]
44. Wu, M.; Zhang, H.; Zhang, X.Y.; Qu, F.Y.; Miao, Y.T. Remote Sensing Quantitative Assessment and Spatial Expansion of Urban Heat Island Effect: A Case Study of Taiyuan. *Remote Sens. Technol. Appl.* **2024**, *39*, 1512–1523.
45. Zhang, Y.; Sheng, Q.; Li, K.; Wang, B.; Li, J.; Ling, X.; Gao, F. Analysis and Reduction of Topographic Effect Induced Errors in Land Surface Temperature Retrieval over the Tibetan Plateau. *Int. J. Appl. Earth Obs. Geoinf.* **2025**, *141*, 104637. [CrossRef]
46. Ye, C.H.; Liu, Y.H.; Liu, W.D.; Liu, C.; Quan, W.J. Research and Application of Remote Sensing Monitoring Indicators for Urban Surface Thermal Environment. *Meteorol. Sci. Technol.* **2011**, *39*, 95–101. [CrossRef]
47. Liu, X.; Zhou, Y.; Yue, W.; Li, X.; Liu, Y.; Lu, D. Spatiotemporal Patterns of Summer Urban Heat Island in Beijing, China Using an Improved Land Surface Temperature. *J. Clean. Prod.* **2020**, *257*, 120529. [CrossRef]

48. Ren, C.Y.; Wu, D.T.; Dong, S.C. Impact of Urbanization on Urban Climate and Environment in Northwest China. *Geogr. Res.* **2006**, 233–241.
49. Kim, S.W.; Brown, R.D. Urban Heat Island (UHI) Variations within a City Boundary: A Systematic Literature Review. *Renew. Sustain. Energy Rev.* **2021**, *148*, 111256. [CrossRef]
50. Liu, K.; Li, X.; Wang, S.; Gao, X. Assessing the Effects of Urban Green Landscape on Urban Thermal Environment Dynamic in a Semiarid City by Integrated Use of Airborne Data, Satellite Imagery and Land Surface Model. *Int. J. Appl. Earth Obs. Geoinf.* **2022**, *107*, 102674. [CrossRef]
51. Chen, X.; Xu, Y.; Yang, J.; Wu, Z.; Zhu, H. Remote Sensing of Urban Thermal Environments within Local Climate Zones: A Case Study of Two High-Density Subtropical Chinese Cities. *Urban Clim.* **2020**, *31*, 100568. [CrossRef]
52. Manoli, G.; Fatichi, S.; Bou-Zeid, E.; Katul, G.G. Seasonal Hysteresis of Surface Urban Heat Islands. *Proc. Natl. Acad. Sci. USA* **2020**, *117*, 7082–7089. [CrossRef]
53. Bu, Z.Q.; Bai, L.B.; Zhang, J.Y. Spatio-temporal Evolution of Urban Agglomerations Along the Yellow River in Ningxia Based on Nighttime Light Remote Sensing. *Remote Sens. Nat. Resour.* **2022**, *34*, 169–176.
54. Mao, H.X.; Jia, K.L.; Gao, X.W.; Zhang, J.H. Spatio-temporal Pattern Analysis of Land Use Change in Yinchuan Plain from 1980 to 2018. *Sci. Technol. Eng.* **2020**, *20*, 8008–8018.

Disclaimer/Publisher's Note: The statements, opinions and data contained in all publications are solely those of the individual author(s) and contributor(s) and not of MDPI and/or the editor(s). MDPI and/or the editor(s) disclaim responsibility for any injury to people or property resulting from any ideas, methods, instructions or products referred to in the content.